

## A Multi-Point Tire Model for Studying Bridge–Vehicle Coupled Vibration

Lu Deng<sup>\*,§</sup>, Ran Cao<sup>†,¶</sup>, Wei Wang<sup>†,||</sup> and Xinfeng Yin<sup>‡,\*\*\*</sup>

*\*Key Laboratory for Wind and  
Bridge Engineering of Hunan Province  
Hunan University, Changsha, Hunan 410082, China*

*†College of Civil Engineering, Hunan University  
Changsha, Hunan 410082, China*

*‡School of Civil Engineering and Architecture  
Changsha University of Science and Technology  
Changsha, Hunan 410004, China*

*§denglu@hnu.edu.cn*

*¶caoran611@gmail.com*

*||jswmw@hnu.edu.cn*

*\*\*\*yinxinfeng@163.com*

Received 5 February 2015

Accepted 24 July 2015

Published 27 August 2015

The contact between a vehicle tire and the road surface has been usually assumed as a single-point contact in the numerical simulation of vehicle–bridge interacted vibrations. In reality, the tire contacts the road surface through a patch instead of a single point. According to some recent studies, the single-point tire model may overestimate the dynamic amplification of bridge responses due to vehicle loadings. A new tire model, namely, the multi-point tire model, is therefore proposed in this paper with the purpose of improving the accuracy of numerical simulation results over the single-point model, while maintaining a certain level of simplicity for applications. A series of numerical simulations are carried out to compare the effect of the proposed tire model with those of the existing single-point model and disk model on the bridge dynamic responses. The proposed tire model is also verified against the field test results. The results show that the proposed multi-point tire model can predict the bridge dynamic responses with better accuracy than the single-point model, especially under distressed bridge deck conditions, and is computationally more efficient and simpler for application than the disk model.

*Keywords:* Dynamic impact factor; single-point tire model; multi-point tire model; disk model; field test.

§Corresponding author.

## 1. Introduction

In recent years, we have seen a growing trend in the application of numerical methods to the study of vehicle–bridge interaction problems. Compared with field studies, numerical simulation provides a convenient and inexpensive tool and is subject to fewer restrictions. Nevertheless, the accuracy of numerical simulation is critical if the results were to have any practical meanings. Thus, much effort has been devoted to developing more accurate numerical models.

In the development of vehicle models, the vehicle tire has been traditionally represented by a point mass with a spring and dashpot, and the vehicle tire and bridge deck were assumed to contact with each other through a single point. This model has been widely used among researchers due to its simplicity.<sup>1–7</sup> However, the accuracy of this model was recently challenged by some researchers.<sup>8,9</sup> Based on the results from a field study, Yin *et al.*<sup>8</sup> found that the single-point model may overestimate the dynamic amplification of the bridge responses, especially under distressed bridge deck conditions. Chang *et al.*<sup>9</sup> also concluded that the single-point tire model tends to induce some unrealistic high-frequency contents to the bridge dynamic responses.

To address these problems, a more authentic tire model, i.e. the disk model, was recently proposed by Yin *et al.*<sup>8</sup> and Chang *et al.*,<sup>9</sup> respectively. The main difference between these two disk models is that the former considers the tire deformation while the latter treats the tire as a rigid disk without deformation. The field test results by Yin *et al.*<sup>8</sup> showed that the disk model predicted bridge responses that match the field measurement much better than the single-point tire model, especially under distressed bridge deck conditions. Chang *et al.*<sup>9</sup> also concluded that the disk model should be adopted in numerical simulations if the velocity and acceleration of the bridge were of major concern. However, the disk model developed by Yin *et al.*,<sup>8</sup> which was based on the theory of dynamics for vehicle tires,<sup>10</sup> requires numerical integration and therefore significant computational effort,<sup>8</sup> while the disk model proposed by Chang *et al.*<sup>9</sup> ignores the deformation of the tire, whose effect deserves further investigation.

This paper presents a new tire model, namely, the multi-point tire model, which takes into account the tire deformation and also considers the simplicity for application. The structure of this paper is organized as follows: First, the bridge–vehicle coupled system is established followed by an introduction of the proposed multi-point tire model. The optimal number of points to be used in the multi-point tire model is then determined based on a parametric study. By adopting the optimal number of points, a series of numerical simulations are then carried out to examine the effect of three different tire models on the bridge dynamic responses. Finally, the proposed tire model is verified against the field test results.

## 2. Analytical Model

### 2.1. Equation of motion of the bridge and vehicle

The equation of motion for the bridge can be expressed as follows:

$$M_b \ddot{d}_b + C_b \dot{d}_b + K_b d_b = F_b, \tag{1}$$

where  $M_b$ ,  $C_b$  and  $K_b$  are the mass, damping, and stiffness matrices of the bridge, respectively;  $d_b$  is the displacement vector of the bridge, and  $\dot{d}_b$  and  $\ddot{d}_b$  are the first and second derivatives of  $d_b$  with respect to time; and  $F_b$  is the vector of wheel-road contact force acting on the bridge.

The equation of motion for a vehicle can be expressed as follows:

$$M_v \ddot{d}_v + C_v \dot{d}_v + K_v d_v = F_G + F_v, \tag{2}$$

where  $M_v$ ,  $C_v$  and  $K_v$  are the mass, damping, and stiffness matrices of the vehicle, respectively;  $d_v$ ,  $\dot{d}_v$  and  $\ddot{d}_v$  are the displacement, velocity, and acceleration vectors of the vehicle, respectively;  $F_G$  is the vector of vehicle gravity force; and  $F_v$  is the vector of wheel-road contact force acting on the vehicle.

### 2.2. Proposed multi-point tire model

In this paper, a new tire model was proposed with the purpose of improving the accuracy of numerical simulations over the single-point model while maintaining certain level of simplicity for its applications. According to the AASHTO LRFD code,<sup>11</sup> the tire-road contact area can be assumed as a single rectangle with a length of 10 inches. Therefore, the proposed multi-point tire model in this study consists of a number of points in contact with the road and spans a length of 25.4 cm (10 inches) in the longitudinal direction. Each of these points is represented by a pair of spring and damper and all points are uniformly distributed in the longitudinal direction. Since the road surface profile is assumed to be identical in the transverse direction, therefore, only one point is used in the transverse direction. A comparison of three different tire models, i.e. the single-point model, disk model,<sup>8</sup> and the proposed multi-point model, is shown in Fig. 1.

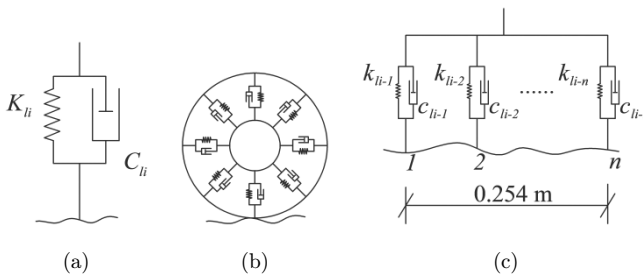


Fig. 1. Three tire models: (a) Single-point model; (b) disk model; (c) multi-point model.

As can be observed from Fig. 1, the multi-point model differs from the single-point model in that the single-point contact between the tire and road in the single-point tire model is replaced by a number of point contacts, each represented by a pair of spring and damper. Based on this, the interaction force between vehicle and bridge can be derived as follows.

First, the interaction force between the tire and bridge deck, denoted as  $F_{v-b}$ , can be calculated as:

$$F_{v-b} = -K_v \cdot \Delta_L - C_v \dot{\Delta}_L, \quad (3)$$

where  $K_v$  and  $C_v$  are the coefficients of the tire spring and damper, respectively; and  $\Delta_L$  is the deformation of the tire spring.

In a vehicle–bridge system, the relationship among the vertical displacement of the tire  $d_v$ , bridge deflection at the contact point  $d_{b\_contact}$ , deformation of the tire spring  $\Delta_L$ , and road surface profile  $r(x)$  can be expressed by the following equation:

$$\Delta_L = d_v - d_{b\_contact} - r(x). \quad (4)$$

Taking the first derivative of Eq. (4) with respect to the time gives:

$$\dot{\Delta}_L = \dot{d}_v - \dot{d}_{b\_contact} - \dot{r}(x). \quad (5)$$

In the proposed multi-point tire model shown in Fig. 1(c), the springs and dampers in the same tire have the same coefficients which are equal to one  $n$ th of the values in the corresponding single-point tire model, where  $n$  is the total number of points in the multi-point model. Therefore, by substituting Eqs. (4) and (5) into Eq. (3), the interaction force acting on the vehicle is obtained as follows:

$$F_{v-b} = -\left(\frac{K_v}{n}\right) \cdot \sum_{i=1}^n (d_{iv} - d_{ib\_contact} - r_i(x)) - \left(\frac{C_v}{n}\right) \cdot \sum_{i=1}^n (\dot{d}_{iv} - \dot{d}_{ib\_contact} - \dot{r}_i(x)), \quad (6)$$

where  $i$  is the point number in the multi-point tire model.

It is noted that the contact area of a real tire will change as the tire–road contact force changes when the truck moves. The disk model can easily deal with this problem because of its circular shape. The proposed tire model deals with this problem based on an equivalent force method which works as follows: When the actual tire–road contact force exceeds the static contact force, the contact area will become larger than its static counterpart (with contact length of 25.4 cm), the springs of the proposed tire model will get further compressed beyond its static equilibrium position, leading to a greater contact pressure. Similarly, when the actual contact pressure/force reduces, the contact area will decrease, so does the pressure in the springs. In this way, the proposed tire model is able to maintain the same contact

force as in the real situation and the vibrations of both the bridge and vehicle will not be affected.

**2.3. Road surface condition**

Road surface condition (RSC) is known as a very important source of excitation for vehicle-induced bridge vibration. A road surface profile is usually assumed to be a zero-mean stationary Gaussian random process. A random road profile can be generated through an inverse Fourier transformation based on a power spectral density (PSD) function such as the one adopted by Dodds and Robson<sup>12</sup>:

$$r(X) = \sum_{k=1}^N \sqrt{2\phi(n_k)\Delta n} \cos(2\pi n_k X + \theta_k), \tag{7}$$

where  $\theta_k$  is a random phase angle which has a uniform distribution from 0 to  $2\pi$ ;  $\phi(\ )$  is the PSD function ( $\text{m}^3/\text{cycle}/\text{m}$ ) for the road elevation; and  $n_k$  is the wave number ( $\text{cycle}/\text{m}$ ). The PSD function used by Huang and Wang<sup>13</sup> was adopted in the present study.

The International Organization for Standardization<sup>14</sup> has proposed a road roughness classification index from A (very good) to E (very poor) according to different values of  $\varphi(n_0)$ . In this study, the classification of road roughness based on the ISO<sup>14</sup> was used. In addition, two-dimensional road roughness profiles, in which the road profile is assumed to be identical throughout the bridge transverse direction, were adopted in this study, as used by many other researchers.<sup>15-17</sup>

**2.4. Equation of motion of the vehicle-bridge coupled system**

For a vehicle moving on a bridge, using the displacement relationship and the interaction force relationship at the contact points, the equations of motion of both the bridge and vehicle can be combined to form a coupled bridge-vehicle system, as shown below:

$$\begin{aligned} & \begin{bmatrix} M_b & \\ & M_v \end{bmatrix} \begin{Bmatrix} \ddot{d}_b \\ \ddot{d}_v \end{Bmatrix} + \begin{bmatrix} C_b + C_{b-b} & C_{b-v} \\ C_{v-b} & C_v \end{bmatrix} \begin{Bmatrix} \dot{d}_b \\ \dot{d}_v \end{Bmatrix} + \begin{bmatrix} K_b + K_{b-b} & K_{b-v} \\ K_{v-b} & K_v \end{bmatrix} \begin{Bmatrix} d_b \\ d_v \end{Bmatrix} \\ & = \begin{Bmatrix} F_{b-r} \\ F_{v-r} + F_G \end{Bmatrix}, \end{aligned} \tag{8}$$

where  $C_{b-b}$ ,  $C_{b-v}$ ,  $C_{v-b}$ ,  $K_{b-b}$ ,  $K_{b-v}$ ,  $K_{v-b}$ ,  $F_{b-r}$  and  $F_{v-r}$  are related to vehicle-bridge interactions and are therefore time-dependent terms. Detailed derivation can be found in Deng.<sup>18</sup>

In this study, the modal superposition technique was used to simplify the equation of motion of the bridge, leading to significantly reduced computational effort. By

doing this, Eq. (8) can then be simplified into the following:

$$\begin{aligned} \begin{bmatrix} I \\ M_v \end{bmatrix} \begin{Bmatrix} \ddot{\xi}_b \\ \ddot{d}_v \end{Bmatrix} + \begin{bmatrix} 2\omega_i \eta_i I + \Phi_b^T C_{b-b} \Phi_b & \Phi_b^T C_{b-v} \\ C_{v-b} \Phi_b & C_v \end{bmatrix} \begin{Bmatrix} \dot{\xi}_b \\ \dot{d}_v \end{Bmatrix} \\ + \begin{bmatrix} \omega_i^2 I + \Phi_b^T K_{b-b} \Phi_b & \Phi_b^T K_{b-v} \\ K_{v-b} \Phi_b & K_v \end{bmatrix} \begin{Bmatrix} \xi_b \\ d_v \end{Bmatrix} = \begin{Bmatrix} \Phi_b^T F_{b-r} \\ F_{v-r} + F_G \end{Bmatrix}. \end{aligned} \quad (9)$$

The fourth-order Runge–Kutta method was adopted to solve Eq. (9) in the time domain. Time histories of both bridge and vehicle responses, including displacement, velocity, and acceleration, can be obtained. For more details of the vehicle–bridge coupled system and the problem-solving process, readers can refer to Ref. 3.

### 3. Numerical Simulations

In this section, numerical simulations will be carried out to compare the proposed multi-point tire model with the two existing models, i.e. the single-point tire model and the disk model previously developed by Yin *et al.*<sup>8</sup> The contents in this section are organized as follows: The bridge and vehicle models, including the RSC, are first introduced; a parametric study is then carried out to determine the optimal number of points to be used in the proposed multi-point model; after that, bridge response time histories obtained from the three different tire models are compared; finally, in order to compare the effect of different tire models on the bridge dynamic responses quantitatively, the dynamic impact factors (IMs) obtained using different tire models are compared.

#### 3.1. Bridge and vehicle models

Three typical simply-supported slab-on-girder concrete bridges, which were designed according to the AASHTO<sup>11</sup> standard specification, were used in the numerical simulations. These three bridges, measuring 9.16 m (short span), 16.76 m (short to medium span), and 39.62 m (long span) in length, respectively, cover a good range of span lengths for this type of bridges. Considering the fact that the vibration of short bridges may be more sensitive to the parameters of vehicle models since the length of the vehicle is close to the span length of short bridges, two bridges with short and short-to-medium spans were selected. For the purpose of convenience, these three bridges are named Bridge 1 (9.16 m), Bridge 2 (16.76 m) and Bridge 3 (39.62 m) hereafter. All three bridges have a roadway width of 9.75 m (32 ft) and bridge deck thickness of 0.20 m (8 in). They all consist of five prestressed concrete girders with a girder spacing of 2.13 m (7 ft), as shown in Fig. 2 where the cross section of Bridge 2 is plotted. More details of the three bridges can be found in Ref. 5.

In this study, a HS20-44 truck, which is the major design truck in the AASHTO code,<sup>11</sup> was adopted as the main vehicle for loading. The analytical model of the truck is shown in Fig. 3. Detailed parameters of the truck model, with coefficients for



Table 1. Major parameters of the HS20-44 truck model.

Items	Parameters	Values
Geometry	L1	1.698 (m)
	L2	2.569 (m)
	L3	1.984 (m)
	L4	2.283 (m)
	L5	2.215 (m)
	L6	2.338 (m)
	b	1.1 (m)
Mass	Truck body 1	2612 (kg)
	Truck body 2	26113 (kg)
	First axle suspension	490 (kg)
	Second axle suspension	808 (kg)
	Third axle suspension	653 (kg)
Moment of inertia	Pitching, truck body1	2022 (kg · m <sup>2</sup> )
	Rolling, truck body 1	8544 (kg · m <sup>2</sup> )
	Pitching, truck body2	33153 (kg · m <sup>2</sup> )
	Rolling, truck body 2	181216 (kg · m <sup>2</sup> )
Spring stiffness Damper coefficient	Upper, first axle	242604 (N/m)
	Lower, first axle	875082 (N/m)
	Upper, second axle	1903172 (N/m)
	Lower, second axle	3503307 (N/m)
	Upper, third axle	1969034 (N/m)
	Lower, third axle	3507429 (N/m)
Damper coefficient	Upper, first axle	2190 (N · s/m)
	Lower, first axle	2000 (N · s/m)
	Upper, second axle	7882 (N · s/m)
	Lower, second axle	2000 (N · s/m)
	Upper, third axle	7182 (N · s/m)
	Lower, third axle	2000 (N · s/m)

in the numerical simulation. Based on the survey results from Lima and de Brito,<sup>21</sup> a 20-mm deep depression located at the entry of the bridge was adopted, as shown in Fig. 4.

The loading position of the vehicle on each bridge is shown in Fig. 2. A total of eight different vehicle speeds, ranging from 15 to 120 km/h with an interval of 15 km/h, were investigated. Three different RSCs were used, namely, good, average, and poor. In order to reduce the bias in the simulation results caused by the randomness of the road surface profile, for each loading condition with a specific RSC, a total of

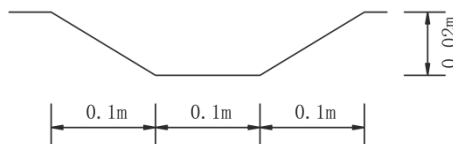


Fig. 4. Depression at the entry of the third bridge span.

20 random road surface profiles were generated. The program was then set to run 20 times using the 20 random road surface profiles, and the average of the 20 impact factors obtained was used in the data analysis.

### ***3.2. Optimal number of points used in the multi-point tire model***

A parametric study was carried out to determine the optimal number of points to be used in the proposed multi-point tire model. A total of eight numbers of points were investigated, namely, 1, 3, 4, 5, 6, 7, 8 and 9. It is noted that the number “1” actually represents the single-point tire model. Again, the total length of the tire-road contact area was set to 25.4 cm (10 inches) according to the AASHTO code.<sup>11</sup> The impact factors of the bridge obtained under three vehicle speeds, namely, 45, 75 and 105 km/h, were used for illustration. The midspan deflection of Girder 4, which had the largest deflection among all five girders, was used for calculating the impact factors for all the three bridges.

Figures 5–7 show the variations of impact factors with the number of points used in the tire model, for the three bridges respectively, when the three-axle vehicle was used. It can be observed from these three figures that: (1) The impact factors obtained from single-point model are considerably larger than those obtained from the multi-point model; (2) the impact factors increase as the RSC becomes worse; (3) the impact factors all start to converge when six points are used in the multi-point tire model, under various cases with different vehicle speeds and road roughness conditions. It is therefore concluded that six points should be used in the multi-point tire model for the three-axle vehicle.

It should be noted that some other observations similar to those observed in Ref. 5 can also be drawn from the figures, but are not discussed here because they are not the focus of this study.

In order to verify whether the optimum number of points used in the tire model of the three-axle vehicle also applies to other vehicle models, the variation of impact factors of Bridge 2 with the number of points used in the tire model of the two-axle vehicle is plotted in Fig. 8. It can be found from Fig. 8 that the impact factors also start to converge with six points used, confirming the results obtained from the three-axle vehicle.

### ***3.3. Bridge dynamic responses obtained using different tire models***

In order to examine the effect of different tire models on the bridge dynamic responses, the response time histories at the midspan of Girder 4 when the three-axle truck travels across Bridge 2 (with depression on the deck) were used for illustration, as plotted in Fig. 9. The vehicle speed was set to 75 km/h.

As can be seen from Fig. 9, the single-point contact tire model induces larger dynamic effect on the bridge responses than the other two tire models. This is especially obvious from Fig. 9(c) that the acceleration obtained from the single-point

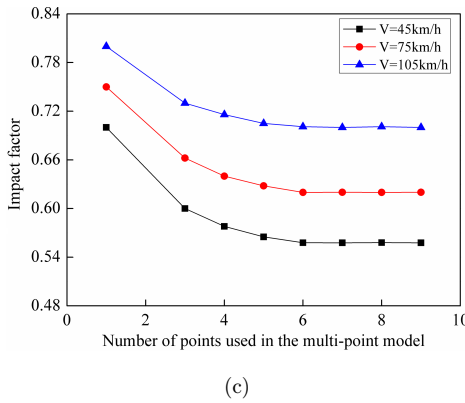
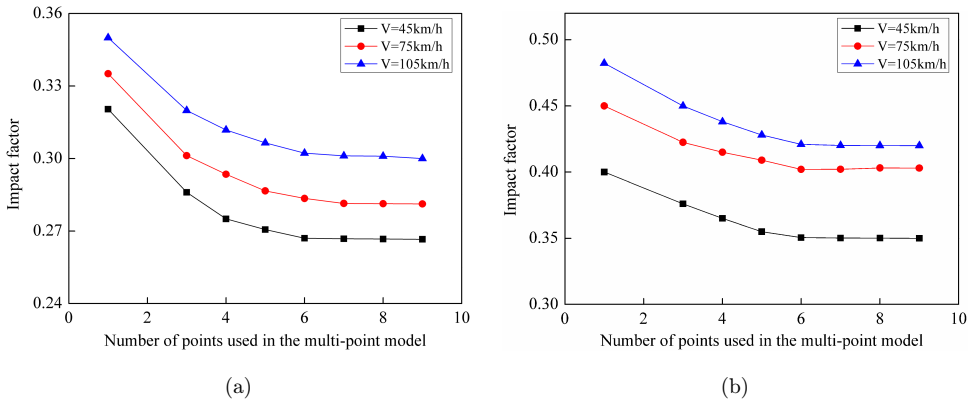


Fig. 5. Effect of number of points in the tire model of the three-axle vehicle on the impact factor of Bridge 1: (a) Good RSC; (b) average RSC and (c) poor RSC.

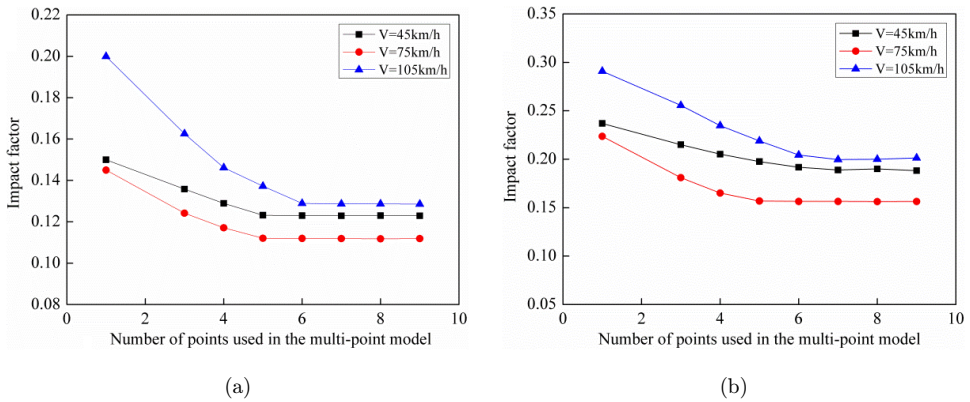
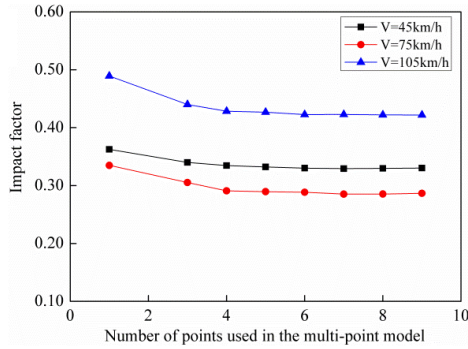
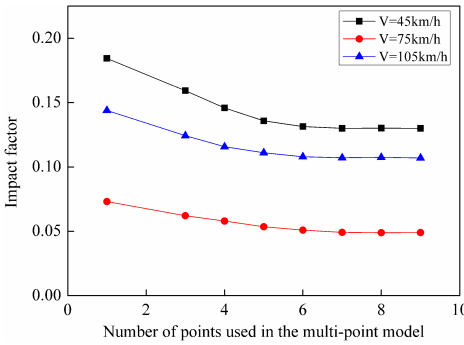


Fig. 6. Effect of number of points in the tire model of the three-axle vehicle on the impact factor of Bridge 2: (a) Good RSC; (b) average RSC and (c) poor RSC.

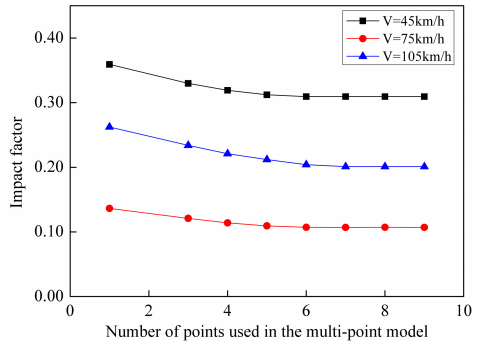


(c)

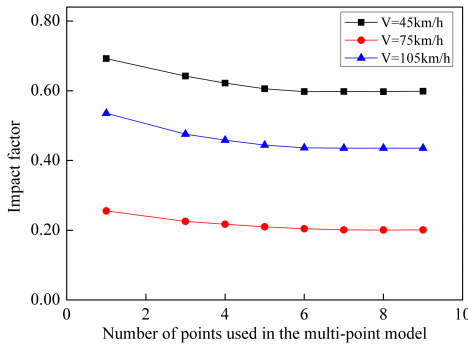
Fig. 6. (Continued)



(a)



(b)



(c)

Fig. 7. Effect of number of points in the tire model of the three-axle vehicle on the impact factor of Bridge 3: (a) Good RSC; (b) average RSC and (c) poor RSC.

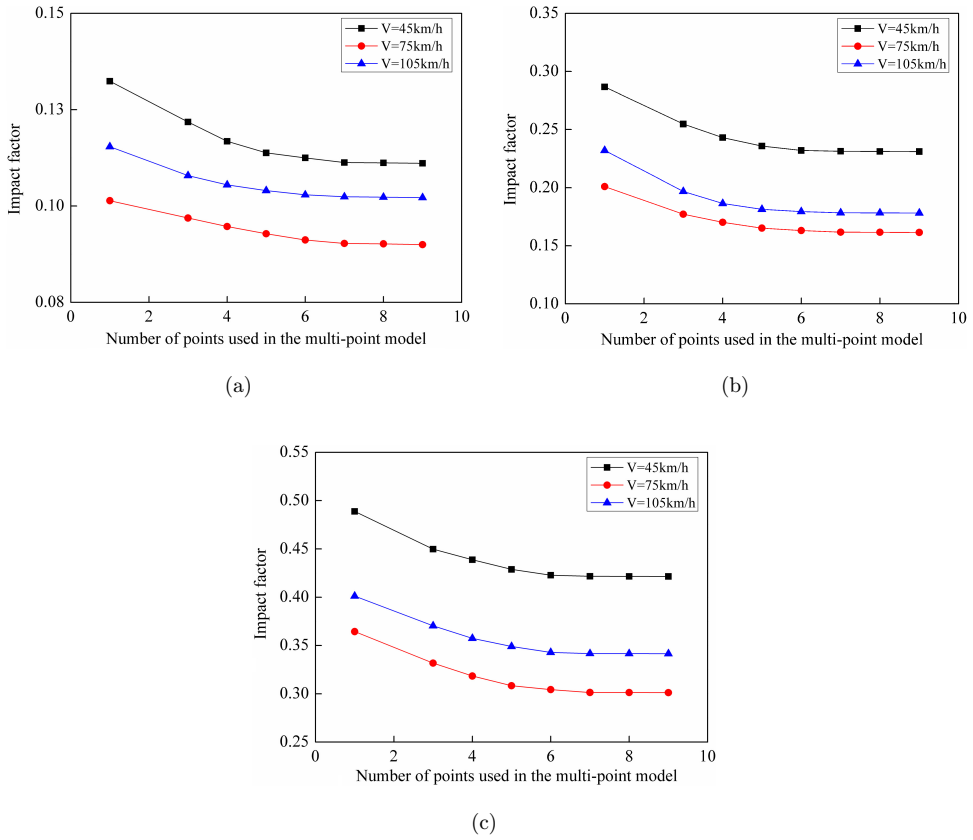


Fig. 8. Effect of number of points in the tire model of the two-axle vehicle on the impact factor of Bridge 2: (a) Good RSC; (b) average RSC and (c) poor RSC.

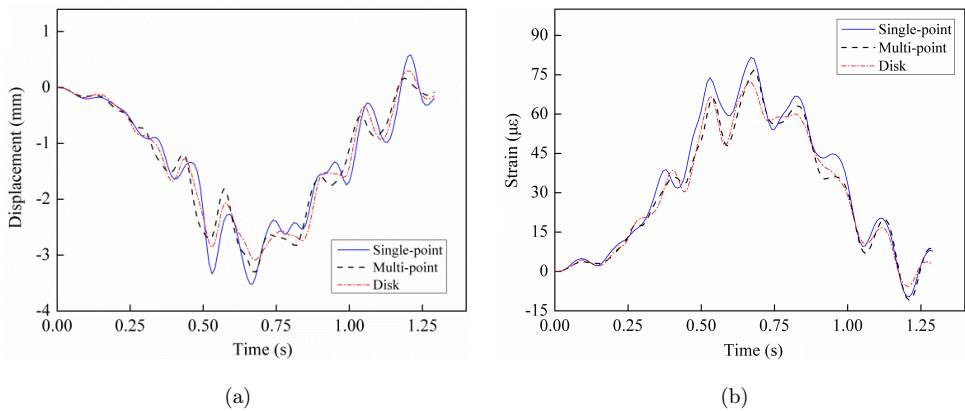
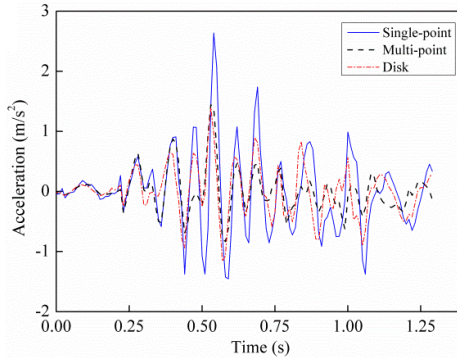


Fig. 9. Bridge response at the midspan of Girder 4: (a) Vertical displacement; (b) longitudinal strain and (c) vertical acceleration.



(c)

Fig. 9. (Continued)

model is much stronger than those obtained using the other two models. It is also observed that the bridge dynamic responses obtained from the multi-point model and disk model are very close while the multi-point model induces slightly larger dynamic effect.

### 3.4. Impact factors obtained using different tire models

Comparisons of the impact factors of Bridge 2 obtained using three different tire models and the three-axle vehicle are illustrated in Fig. 10. Again, three RSCs and eight vehicle speeds were considered. As can be seen from Fig. 10, the impact factors obtained using the three different tire models follow the same trend with the change of vehicle speed under all three RSCs. However, it is also observed that an increase of vehicle speed does not necessarily lead to an increase of impact factors. This phenomenon has also been observed by many other researchers.<sup>5,17</sup> It is generally believed that the resonance between the bridge and vehicle contributes to the large impact factors at certain vehicle speeds.<sup>22</sup> It is also observed that the impact factors obtained using the proposed multi-point model and the disk model are almost identical while they are both slightly smaller than the values obtained using the single-point model.

In a previous study by Yin *et al.*,<sup>8</sup> it was found that the single-point model may overestimate the dynamic amplification of bridge responses, especially under distressed bridge deck conditions. Therefore, a distressed bridge deck condition (Fig. 4) was also studied.

Figure 11 shows the comparisons of the impact factors of Bridge 2 obtained using three different tire models under the distressed bridge deck condition and the action of the three-axle vehicle. As can be seen from the comparison between Figs. 10 and 11, similar trends were observed between the results obtained for cases with and without depression on the bridge deck. However, it is also noticed that with the

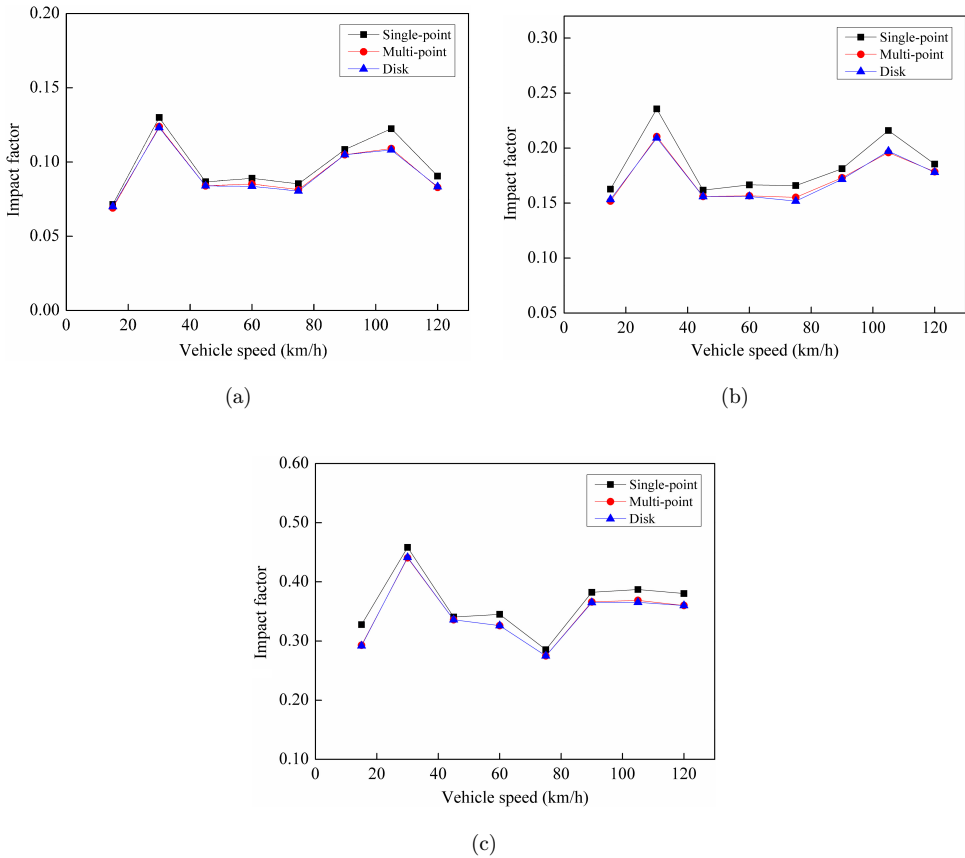


Fig. 10. Impact factors under different vehicle speeds without depression on the bridge deck: (a) Good RSC; (b) average RSC and (c) poor RSC.

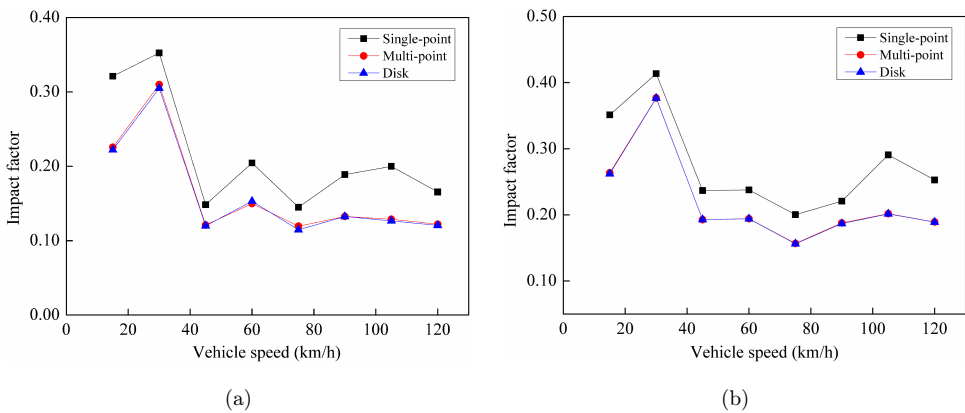
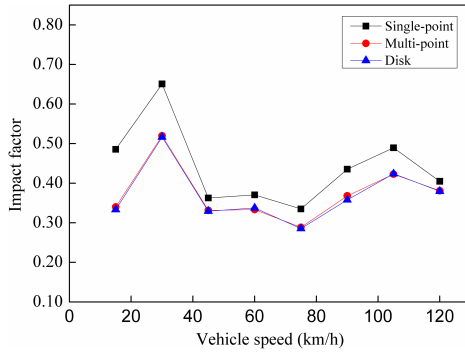


Fig. 11. Impact factors under different vehicle speeds with depression on the bridge deck: (a) Good RSC; (b) average RSC and (c) poor RSC.



(c)

Fig. 11. (Continued)

depression present at the bridge entry, the dynamic impact factors obtained using the single-point model are significantly larger than those obtained using the other two models, with the largest difference reaching 0.1. These results confirmed the conclusion by Yin *et al.*<sup>8</sup>

#### 4. Verification by Field Study

##### 4.1. Test bridge

The test bridge is located over the Cypress Bayou in District 61, Louisiana. The bridge has three straight simple-supported spans, each measuring 16.76 m (55 ft) in length, as shown in Fig. 12. The bridge consists of seven AASHTO Type II pre-stressed concrete girders with girder spacing of 2.13 m (7 ft). Since all three spans of



Fig. 12. The test bridge in Louisiana.

the bridge are simply-supported, only the third span of the bridge was selected for testing. All seven girders of the third span were instrumented with strain gauges, accelerometers, and cable extension transducers, which were placed at the bottom of the midspan of the girders.

Based on the configuration of the bridge, a finite element model was created for the selected bridge span using the ANSYS program. The bridge deck, girders, diaphragms, shoulder, and railing were modeled using solid elements with three translational degrees-of-freedom (DOF) for each node. The rubber bearings were modeled using equivalent beam elements with six DOFs (three translational and three rotational) for each node. The finite element bridge model was updated using field measured bridge responses before being used in the numerical simulation. More details of the finite element model of the test bridge can be found in Ref. 23.

#### 4.2. Test truck

The test truck used in the field testing was a dump truck with a single front axle and a two-axle group for the rear (Fig. 13). The static loads for the front, middle, and rear axles of this truck are 80.0, 95.6 and 95.6 kN, respectively. The distances from the middle axle to the front and rear axles are 6.25 and 1.2 m, respectively. An analytical model for this test truck was created, as shown in Fig. 14. It should be noted that Fig. 14 only shows the truck model with single-point tire models. More details, including the parameters for the test truck, can be found in Ref. 24.

In the numerical simulations presented in the following sections, the effects of the three tire models will be compared. Based on the parametric study in the previous section, six points were used in the multi-point tire model.



Fig. 13. The test truck used in the field testing.

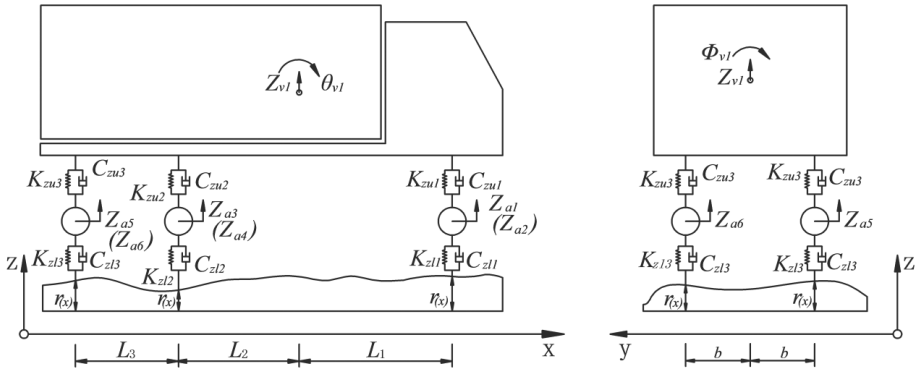


Fig. 14. The analytical model for the test truck (with single-point tire model).

### 4.3. Road surface profile

The road surface profile of the bridge deck was measured by a laser profiler, which obtains the longitudinal road surface profile along the wheel tracks. A two-dimensional road surface profile was used in this paper. In order to check the performance of the proposed tire model under distressed bridge deck conditions, a wood bump with a height of 1.5-inch was placed at the entry of the bridge span of interest. Figure 15 shows the measured road surface profile with the wood bump present at the entry of the third bridge span.

### 4.4. Loading cases

Two loading cases were investigated in the field testing. Figure 16 shows the loading positions of the truck for the two cases. In both loading cases, the truck was set to travel across the bridge at a speed of 64.4 km/h (40 mph).

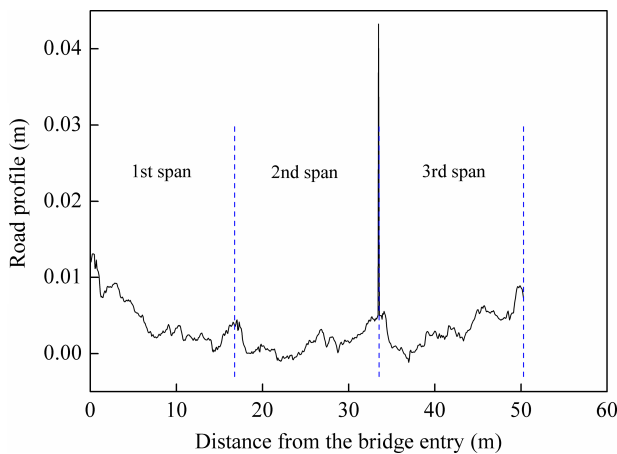


Fig. 15. The measured road roughness profile with the wood bump present.

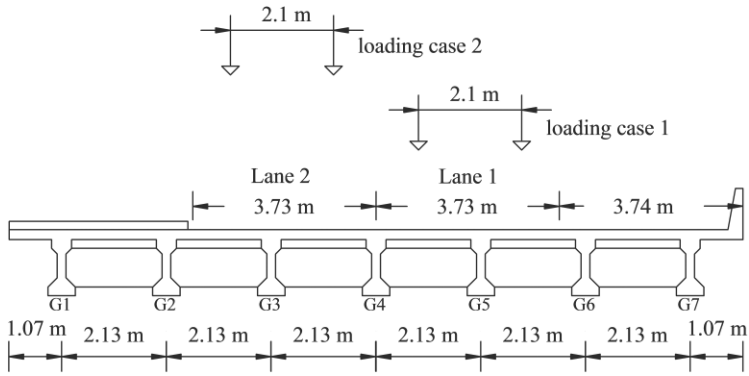


Fig. 16. Bridge cross section and loading position of the truck.

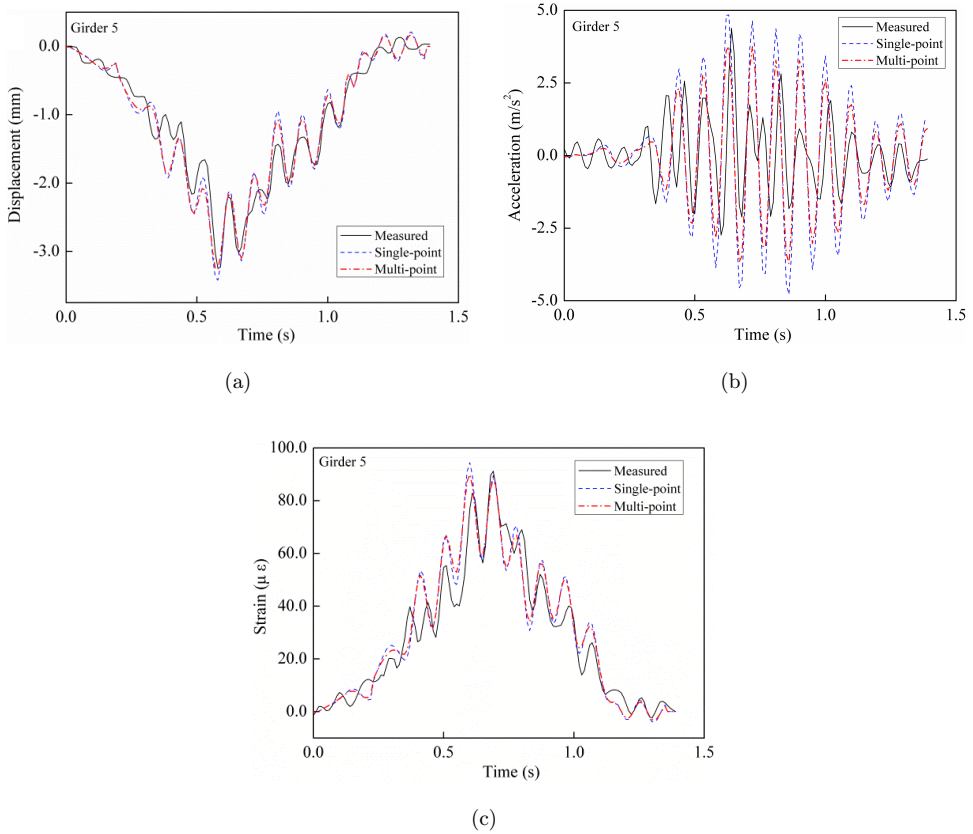


Fig. 17. Bridge responses for loading case 1: (a) Vertical displacement; (b) vertical acceleration and (c) longitudinal strain.

4.5. Test results

For both loading cases, comparisons were made between the bridge responses, including the vertical deflection, vertical acceleration, and longitudinal strain, obtained from field measurement and numerical simulation. For each loading case, the bridge responses of the girder carrying the largest amounts of loads, i.e. Girder 5 for loading case 1 and Girder 3 for loading case 2, were selected for illustration in this section.

For loading case 1, the comparison between the field measured and simulated bridge responses, including midspan vertical displacement, vertical acceleration, and longitudinal strain, using the two different tire models are plotted in Fig. 17 while the results for loading case 2 are plotted in Fig. 18.

From Figs. 17 and 18, it can be observed that: (1) The simulated bridge responses obtained using both tire models match the field measurements very well; (2) the proposed multi-point contact tire model predicts bridge responses with smaller dynamic effects which generally match the field measurements better than the

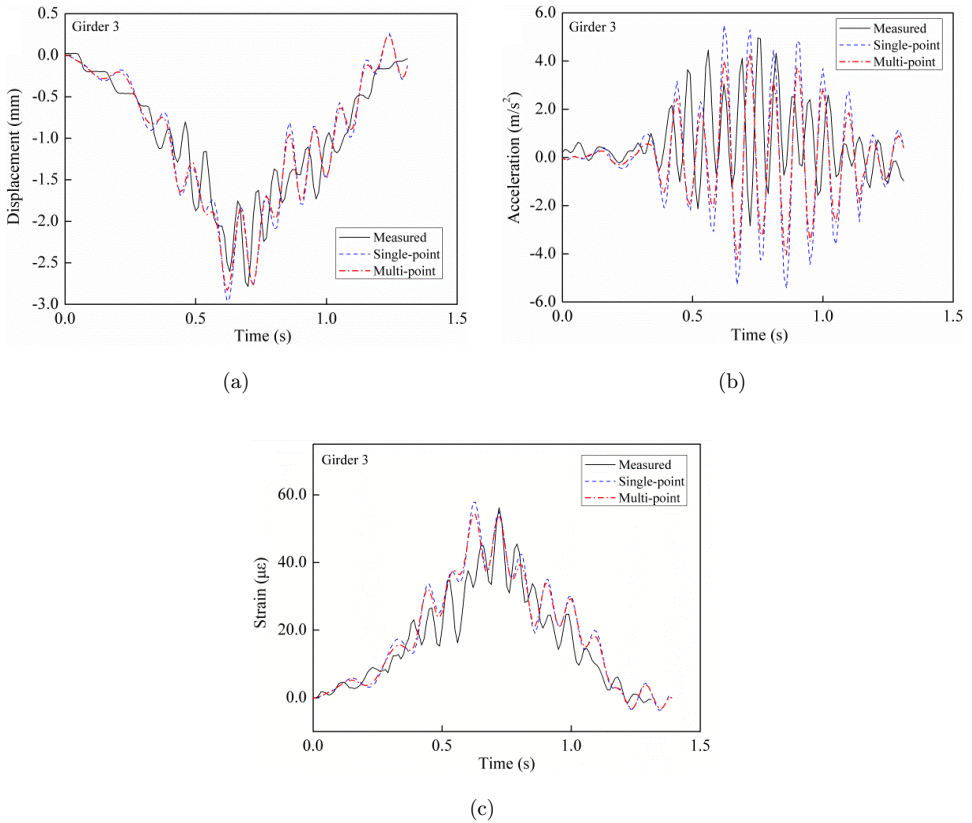


Fig. 18. Bridge responses for loading case 2: (a) Vertical displacement; (b) vertical acceleration and (c) longitudinal strain.

Int. J. Str. Stab. Dyn. Downloaded from www.worldscientific.com by UNIVERSITY OF IOWA on 09/16/15. For personal use only.

single-point contact tire model, especially for the acceleration responses. These observations generally agree with those made from the numerical simulations in the previous section. These results also suggest that the multi-point tire model should be adopted if the acceleration is of major concern.

It should be noted that both measured acceleration time histories in Figs. 17(b) and 18(b) seem to have shifted (from the expected values) to the positive side to some degree, as can be seen from the fact that the maximum positive acceleration, in both figures, is larger than the maximum negative acceleration. In fact, the maximum positive and negative accelerations can usually be expected to be close in practice. This is due to the system calibration error, as can be supported by the fact that the acceleration time history in Fig. 18(b) has slightly shifted to the positive side from the very beginning. This factor should be taken into account in order to draw a fair comparison between the simulated and measured accelerations.

## 5. Conclusion

A new multi-point tire model was developed for studying the bridge–vehicle coupled vibration. The optimal number of points to be used in this new tire model was determined based on a parametric study. The multi-point tire model was then compared to the existing single-point tire model and disk model using numerical simulations. Field tests were also conducted and the proposed new tire model was verified against field measurements. The following conclusions can be reached based on the results from this study:

- When a contact length of 25.4 cm (10 inches), as recommended by the AASHTO code, was adopted in the proposed tire model, the use of six points in the proposed tire model will achieve good convergence and accuracy for the bridge dynamic responses due to moving vehicles.
- The proposed multi-point tire model produces more accurate results with smaller dynamic effects than the single-point tire model, especially under distressed bridge deck conditions. However, it should be noted that for well-maintained RSCs, there is no significant difference between the impact factors obtained using the two different tire models.
- Compared with the disk model, the proposed multi-point tire model can produce results with the same level of accuracy. However, the multi-point model is much simpler and more convenient to use because integration is not required in calculating the wheel force and solving the equation of motion.
- A comparison between the simulated and field measured bridge responses showed that for the case with a wood bump present at the bridge entry, the simulated bridge responses obtained from the proposed multi-point model match the field measurements better than those obtained from the single-point model, especially for the bridge acceleration. These results demonstrate the need of using more realistic tire models, such as the disk model and the proposed multi-point model,

for distressed bridge deck conditions and when bridge acceleration is of major concern.

## Acknowledgments

This work was supported by the National Natural Science Foundation of China (Grant Nos. 51208189 and 51478176) and Excellent Youth Foundation of Hunan Scientific Committee (Grant No. 14JJ1014).

## References

1. D. Z. Huang, T. L. Wang and M. Shahawy, Impact analysis of continuous multigirder bridges due to moving vehicles, *J. Struct. Eng.* **118**(12) (1992) 3427–3443.
2. Y. B. Yang, S. S. Liao and B. H. Lin, Impact formulas for vehicles moving over simple and continuous beams, *J. Struct. Eng.* **121**(11) (1995) 1644–1650.
3. S. S. Law and X. Q. Zhu, Bridge dynamic responses due to road surface roughness and braking of vehicle, *J. Sound. Vibr.* **282**(3–5) (2005) 805–830.
4. E. J. O'Brien, D. Cantero, B. Enright and A. González, Characteristic dynamic increment for extreme traffic loading events on short and medium span highway bridges, *Eng. Struct.* **32**(12) (2010) 3827–3835.
5. L. Deng and C. S. Cai, Development of dynamic impact factor for performance evaluation of existing multi-girder concrete bridges, *Eng. Struct.* **32**(1) (2010a) 21–31.
6. Y. B. Yang, M. C. Cheng and K. C. Chang, Frequency variation in vehicle–bridge interaction systems, *Int. J. Struct. Stab. Dynam.* **13**(2) (2013) 1350019.
7. Y. Li, S. Zhu, C. Cai, C. Yang and S. Qiang, Dynamic response of railway vehicles running on long-span cable-stayed bridge under uniform seismic excitations, *Int. J. Struct. Stab. Dynam.* **16** (2016) 1550005.
8. X. F. Yin, C. S. Cai, Z. Fang and L. Deng, Bridge vibration under vehicular loads — Tire patch contact versus point contact, *Int. J. Struct. Stab. Dynam.* **10**(3) (2010) 529–554.
9. K. C. Chang, F. B. Wu and Y. B. Yang, Disk model for wheels moving over highway bridges with rough surfaces, *J. Sound. Vibr.* **330** (2011) 4930–4944.
10. G. Gim and P. E. Nikraves, Analytical model of pneumatic types for vehicle dynamic simulations Part 2: Comprehensive slips, *Int. J. Vehicle. Des.* **12**(1) (1991) 19–39.
11. American Association of State Highway and Transportation Officials (AASHTO), AASHTO LRFD Bridge Design Specifications, Washington, D.C. (2012).
12. C. J. Dodds and J. D. Robson, The description of road surface roughness, *J. Sound. Vibr.* **31**(2) (1993) 175–183.
13. D. Z. Huang and T. L. Wang, Impact analysis of cable-stayed bridges, *Comput. Struct.* **43**(5) (1992) 897–908.
14. ISO (International Organization for Standardization), Mechanical Vibration–Road Surface Profiles–Reporting of Measured Data, ISO 8068 (1995).
15. D. Huang, T. L. Wang and M. Shahawy, Vibration of horizontally curved box girder bridges due to vehicles, *Comput. Struct.* **68**(5) (1998) 513–528.
16. W. Guo and Y. Xu, Safety analysis of moving road vehicles on a long bridge under crosswind, *J. Eng. Mech.* **132**(4) (2006) 438–446.
17. X. M. Shi, C. S. Cai and S. R. Chen, Vehicle induced dynamic behavior of short span bridges considering effect of approach span condition, *J. Bridge. Eng.* **13**(1) (2008) 83–92.
18. L. Deng, System identification of bridge and vehicles based on their coupled vibration, Ph.D. thesis, Baton Rouge (LA): Louisiana State University, USA (2009).

19. Y. L. Xu and W. H. Guo, Dynamic analysis of coupled road vehicle and cable-stayed bridge systems under turbulent wind, *Eng. Struct.* **25**(4) (2003) 473–486.
20. Y. Zhang, C. S. Cai, X. Shi and C. Wang, Vehicle-induced dynamic performance of FRP versus concrete slab bridge, *J. Bridge. Eng.* **11**(4) (2006) 410–419.
21. J. M. Lima and J. de Brito, Inspection survey of 150 expansion joints in road bridges, *Eng. Struct.* **31** (2009) 1077–1084.
22. L. Deng, Y. Yu, Q. L. Zou and C. S. Cai, State-of-the-art review on dynamic impact factors of highway bridges, *J. Bridge. Eng.* (2014), 10.1061/(ASCE)BE.1943-5592.0000672, 04014080.
23. L. Deng and C. S. Cai, Bridge model updating using response surface method and genetic algorithm, *J. Bridge. Eng.* **15**(5) (2010b) 553–564.
24. C. S. Cai, X. M. Shi, M. Araujo and S. R. Chen, Effect of approach span condition on vehicle-induced dynamic response of slab-on-girder road bridges, *Eng. Struct.* **29** (2010) 3210–3226.